Amyloid β oligomers constrict human capillaries in Alzheimer's disease via signaling to pericytes

Ross Nortley[1], **Nils Korte**[#1], **Pablo Izquierdo**[#1], **Chanawee Hirunpattarasilp**[#1], **Anusha Mishra**[#2], **Zane Jaunmuktane**[#3,4], **Vasiliki Kyrargyri**[#1,%], **Thomas Pfeiffer**[1], **Lila Khennouf**[1], **Christian Madry**[1,&], **Hui Gong**[1], **Angela Richard-Loendt**[3], **Wenhui Huang**[5], **Takashi Saito**[6], **Takaomi C. Saido**[6], **Sebastian Brandner**[3,7], **Huma Sethi**[8], **David Attwell**[1,+]

[1]Dept. of Neuroscience, Physiology & Pharmacology, University College London, Gower Street, London, WC1E 6BT, UK

[2]Knight Cardiovascular Institute, Oregon Health & Science University, 3181 SW Sam Jackson Park Rd, Portland, OR 97239, USA

[3]Division of Neuropathology, National Hospital for Neurology and Neurosurgery, Queen Square, London WC1N 3BG, UK

[4]Dept. of Clinical and Movement Neurosciences, UCL Queen Square Institute of Neurology, Queen Square, London WC1N 3BG, UK

[5]Molecular Physiology, CIPPM, University of Saarland, D-66421, Homburg, Germany

[6]Laboratory for Proteolytic Neuroscience, RIKEN Centre for Brain Science, Wako, Saitama, 351-0198, Japan

[7]Dept. of Neurodegenerative Disease, UCL Institute of Neurology, Queen Square, London WC1N 3BG, UK

[8]Division of Neurosurgery, UCL Institute of Neurology, Queen Square House, London WC1N 3BG, UK

[+]Address correspondence to David Attwell: d.attwell@ucl.ac.uk.
[%]Current address: Hellenic Pasteur Institute, Athens, Greece.
[&]Current address: Charité-Universitätsmedizin, Berlin, Germany.

[#] These authors contributed equally to this work.

Abstract

Cerebral blood flow is reduced early in Alzheimer's disease (AD). Because most of the vascular resistance within the brain is in capillaries, this could reflect dysfunction of contractile pericytes on capillary walls. Here we used live and rapidly-fixed biopsied human tissue to establish disease-relevance, and rodent experiments to define mechanism. We found that, in humans with cognitive decline, amyloid β (Aβ) constricts brain capillaries at pericyte locations. This was caused by Aβ generating reactive oxygen species, which evoked the release of endothelin-1 (ET) that activated pericyte ET_A receptors. Capillary, but not arteriole, constriction also occurred in vivo in a mouse model of AD. Thus, inhibiting the capillary constriction caused by Aβ could potentially reduce energy lack and neurodegeneration in AD.

Vascular compromise occurs early in Alzheimer's disease (AD) (1, 2). Cerebral blood flow in the grey matter can be reduced by over 40% (3), and indeed reduced cerebral blood flow is the earliest biomarker of the development of the disease (1). Around the time that the amyloid hypothesis for Alzheimer's Disease (AD) was proposed (4–6), it was reported that capillaries in the brains of AD patients showed an abnormal focally-constricted morphology (7). Although much succeeding work focused on Aβ- and tau-evoked damage to neurons, increasing evidence suggests a role for vascular disturbance in the onset of AD (8, 9). Exogenous amyloid β can reduce cerebral blood flow (10–12), and reduced blood flow increases Aβ production (13, 14).

Investigations of the vascular effects of exogenous Aβ have focused on arteries and arterioles (12, 15), but the majority of the vascular resistance within the brain is located in capillaries (16). Capillary dysfunction correlates with cognitive decline in AD (17). This suggests that capillaries could be the most important locus where Aβ produced within the brain can act to decrease cerebral blood flow. A subset of pericytes on capillary walls is contractile (these are the only contractile cells on capillaries (18)) and can alter cerebral blood flow by adjusting their contractile tone (18–20). In a rodent model of AD there are disturbances of unknown origin in the control of capillary blood flow (21). We therefore investigated how pericytes were affected by exogenous and endogenously generated Aβ, and in particular by $Aβ_{1–42}$ oligomers, the molecular species believed to be responsible for Aβ's toxic effects in AD (22, 23). To maximise the relevance to human disease, we used living human brain slices derived from neurosurgically-resected brain tissue to study acute responses to Aβ, and rapidly-fixed human brain biopsy tissue (from living patients with or without Aβ deposition) to assess pericyte responses to long-term accumulation of endogenous Aβ in AD. The effects seen in human tissue were also seen in vivo in a transgenic mouse model of AD and were analysed mechanistically in brain slices.

Amyloid β constricts human capillaries at pericytes

Living human brain cortex slices were obtained from tissue removed during neurosurgical operations to access tumours (see Materials and Methods) and either fixed for immunohistochemistry or imaged live to study pericyte properties. Labeling the basement

membrane with fluorescently-tagged isolectin B_4, or immunolabeling for the pericyte marker platelet-derived growth factor receptor β (PDGFRβ), revealed pericyte morphology. Pericytes were observed with a classical "bump-on-a-log" morphology on the straight parts of capillaries, or at their branch points, with processes extending along and around the capillaries (Fig. 1A, B). With experience, morphology alone was sufficient to identify pericytes reliably in brain slices (Fig. S1). The mean distance between human pericytes was 65.3 ± 0.4 μm (for 94 pericytes imaged in tissue from 2 patients), 30% larger than in rodents (19). As for arteriole smooth muscle cells (Fig. 1C), the processes of 36% of pericytes labeled for α smooth muscle actin (Fig. 1D) and the real percentage may be significantly higher with different fixation techniques (24), providing a mechanistic basis for the Aβ-evoked contraction described below. In human brain slices, as previously reported for rodent capillaries (18, 19), superfused noradrenaline constricted and glutamate dilated the capillaries at pericyte locations (Fig. 1E, F). This is consistent with the circumferential processes of pericytes (which are oriented to be able to reduce capillary diameter) being preferentially found near pericyte somata (Fig. S2) so that capillary constriction by pericytes occurs predominantly near these somata (Fig. S3). Thus, the surgery-derived human tissue had functioning contractile pericytes (Fig. 1E-F).

Aβ was oligomerised (see Materials and Methods), and silver staining of SDS-PAGE gels was used to assess the degree of aggregation of the Aβ isoforms. The predominant species produced (other than monomers) for $A\beta_{1-42}$ and $A\beta_{1-40}$ had a molecular weight of 2 to 4 times that of monomers, whereas scrambled $A\beta_{1-42}$ formed mainly monomers (Fig. 1G). Applying soluble $A\beta_{1-42}$ (oligomeric + monomeric, 72 nM calculated from the monomeric MW) to human brain slices evoked a slowly developing constriction of all 4 capillaries tested, which reduced their diameter by ~25% after 40 mins (Fig. 1H, significantly reduced, p=0.01).

Because the limited availability of live human tissue precluded detailed analysis of the mechanism underlying the Aβ-evoked constriction, we carried out experiments on rat cortical slices. As for human capillaries, $A\beta_{1-42}$ evoked a constriction of rat capillaries near pericyte locations that was visible using either bright field illumination or two-photon fluorescence imaging of isolectin B_4 (Fig. 2A-C, G). Of 20 capillaries tested, 16 (80%) showed a >5% constriction in response to $A\beta_{1-42}$. The time course of the mean $A\beta_{1-42}$-evoked constriction (including all vessels) was similar (Fig. 2C) to that in human cortex (Fig. 1H), reaching ~15% after 1 hour (p=0.006). $A\beta_{1-40}$ also evoked a similar constriction (Fig. 2C, G; p=0.048) in 5 out of 6 capillaries tested (83%). Capillaries monitored for an hour without applying Aβ, or those to which a version of $A\beta_{1-42}$ with a scrambled sequence was applied (prepared as for the Aβ oligomers), showed no significant diameter change (Fig. 2C, G). Scrambled $A\beta_{1-42}$ mainly forms monomers (Fig. 1G, and see Materials and Methods), unlike $A\beta_{1-42}$ and $A\beta_{1-40}$, which may indicate that oligomer formation is obligatory for an effect on pericytes. The pericyte-mediated constriction evoked by $A\beta_{1-42}$ showed a Michaelis-Menten dependence on Aβ concentration, with an apparent EC_{50} (K_m) of 4.7 nM (Fig. 2D).

Reactive oxygen species and endothelin-1 generate the capillary constriction

The $A\beta_{1-42}$-evoked capillary constriction in rat cortical slices was blocked by the endothelin-1 (ET) type A receptor blocker BQ-123 (1 μM, p=0.008, Fig. 2E, G), by application of superoxide dismutase 1 (SOD1, 150 units/ml, p=3.7×10^{-6}, Fig. 2E, G) which scavenges reactive superoxide generated when Aβ activates NADPH oxidase (and prevents hydroxyl radical formation by the Fenton reaction), or by inhibiting NADPH oxidase with diphenyleneiodonium (DPI, 10 μM, p=0.032, Fig. 2F, G). In contrast, applying these agents alone did not affect capillary diameter (changes after 1 hour were: BQ-123, -0.7±5.2%, n=13, p=0.9; SOD1, 3.4±5.8%, n=9, p=0.57; DPI, -7.4±3.2%, n=5, p=0.082). The $A\beta_{1-40}$-evoked capillary constriction was also abolished by BQ-123 (a 6.2±1.6% dilation was seen after 1 hour of $A\beta_{1-40}$ applied in BQ-123, n=5), contradicting the suggestion (25) that $A\beta_{1-40}$ does not evoke endothelin release. These results suggest the involvement of NADPH oxidase-mediated reactive oxygen species (ROS) generation and ET release in the Aβ-evoked capillary constriction. Reactive nitrogen species derived from superoxide were not involved, because inhibiting nitric oxide synthase (NOS) with L-NNA (100 μM) had no effect (p=0.83) on the Aβ-evoked constriction (Fig. 2F, G; L-NNA alone had no effect: after 1 hour the diameter change was -0.5±7.9%, n=6, p=0.99). The fact that Aβ evoked constrictions even in the presence of L-NNA also rules out the possibility that Aβ-evoked ROS production caused constriction (26) by ROS binding to, and removing, vasodilatory NO. The NOX4 blocker GKT137831 (0.45 μM) abolished the Aβ-evoked capillary constriction (Fig. 2F, G; p=0.0011, but did not affect diameter when applied alone: changed by 5.7±5.6%, n=6, p=0.35 after 1 hour), whereas the NOX2 blocker ebselen (2 μM) reduced the constriction by only 45% (n=8, p=0.027; on its own ebselen had no effect: diameter changed by 1.4%±3.8%, n=9, p=0.8 after 1 hour). These data suggest that NOX4 in pericytes or endothelial cells (27–29), rather than NOX2 in immune cells (28, 29), is the NADPH oxidase mainly responsible for generating the reactive oxygen species (ROS) that evoke capillary constriction. Data presented below in Fig. 3 suggest that the NOX4 producing the ROS is in pericytes.

To confirm that pericytes constrict in response to activation of ET receptors, we applied ET (10 nM) either alone or with a blocker of its type A (ET_A) or type B (ET_B) receptors. Endothelin-1 evoked a strong (>65%) pericyte-mediated constriction of capillaries (p=2×10^{-12}), which was blocked by the ET_A blocker BQ-123 (1 μM, p=2.6×10^{-11}), but not by the ET_B blocker BQ-788 (1 μM, p=0.91, Fig. 2H). ET still evoked a constriction in the presence of SOD1 (p=1.3×10^{-8}, Fig. 2I) implying that ET acts downstream of ROS, while generating ROS using H_2O_2 (1 mM) evoked a constriction (p=1.1×10^{-5}) that was reduced by BQ-123 (p=0.009, Fig. 2J), suggesting that ROS evoke constriction via ET_A receptor activation. Consistent with the ET_A receptors that generate pericyte contraction being on the pericytes themselves, we found that, in pericytes expressing GCaMP5G (see Materials and Methods), applying ET (10 nM) evoked a rise in $[Ca^{2+}]_i$ while aCSF had no effect (Fig. 2K-L). These data establish $A\beta_{1-42}$-evoked generation of ROS as being upstream of the elevated level (30, 31) (or potentiated effect (32)) of ET that makes pericytes constrict capillaries.

In profound ischemia, pericyte-evoked constriction of capillaries is followed by the pericytes dying necrotically in rigor (caused by an excessive rise of $[Ca^{2+}]_i$), thus maintaining a decreased capillary diameter and a long-lasting decrease of blood flow (19). Pericytes also die after accumulating Aβ in AD (33). We assessed whether exposure to 1.4 μM soluble Aβ$_{1-42}$ or 100 nM ET for 3 hours had a similar effect on pericyte health, by applying propidium iodide to label cells with membranes that had become non-specifically permeable, as occurs in ischemia (19). These treatments did not significantly increase pericyte death on this time scale (Fig. 2M, p=0.85 for Aβ$_{1-42}$ and 0.59 for ET).

To assess which cell types generated ROS in response to Aβ, in brain slices we employed imaging of the ROS sensor dihydroethidium, which generates fluorescence when oxidised dihydroethidium intercalates into DNA (see Materials and Methods). Aβ$_{1-42}$ (72 nM, applied for 40 mins) evoked an increase in ROS level that was suppressed by the presence of SOD1 (Fig. 3A, B). Previous work has suggested that ROS can be generated in response to Aβ by resident microglia (34) or perivascular macrophages (35), but the cells showing the brightest oxidised dihydroethidium fluorescence were located on capillaries, had the morphology of pericytes, and labeled for NG2 but not Iba1 (Fig. 3C), implying that they are pericytes. The ROS signal generated in regions of interest placed over the nuclei of NG2-expressing cells on capillaries (pericytes), or of Iba1-labeled immune cells, was quantified in 6 image stacks (1 stack/slice) from slices not exposed to Aβ (containing a total of 128 pericytes and 238 Iba1-labeled cells) and 8 stacks from slices exposed to Aβ (containing 171 pericytes and 270 Iba1-labeled cells). Aβ increased ROS production in pericytes by a factor of 7.28 (p=0.001) and in immune (Iba1-expressing) cells by a factor of 1.76 (p=0.05). Taking into account the different numbers and basal ROS production of pericytes and immune cells revealed that Aβ evoked 6.4-fold more total ROS generation by pericytes than by immune cells (Fig. 3D). This is consistent with the data above (Fig. 2F, G) suggesting that NOX4 in pericytes (27–29) is the main generator of the ROS involved in constricting capillaries early in the response to Aβ.

To confirm that both pericytes and microglia generate ROS in response to Aβ, in brain slices we fluorescently imaged the level of reduced glutathione (GSH, see Materials and Methods), which is consumed as it scavenges ROS. Aβ (72 nM for 40 mins) reduced the GSH level in pericytes by 20% and in microglia by 55% (Fig. S4, p=0.014 and p=$2x10^{-29}$ respectively). These changes cannot be converted to ROS synthesis rates because they will be affected by GSH regeneration rate, which may differ in microglia and in pericytes.

Pericytes constrict capillaries in human cognitive decline patients with Aβ deposition

Because acute exposure to Aβ cannot mimic the slow increase that occurs over decades in human AD patients, we studied rapidly-fixed brain cortical biopsy tissue from living patients being investigated for cognitive decline of unknown cause (for demographics, biopsy and tissue processing details, see Materials and Methods). Tissue sections were labeled with antibodies recognising residues 8-17 of Aβ (lower panels of Fig. 4A-B) and PDGFRβ (upper panels of Fig. 4A-B). Of 13 patients, 7 turned out to have Aβ deposition while 6 did

not. Pericytes were readily identifiable from their PDGFRβ labeling. Averaging over 120-140 adjacent fields of view (400 μm square in size, randomly placed on each section as a 5x4 grid of squares) in tissue from the two types of patient, with the experimenter blinded to the occurrence of Aβ deposition (viewing only the PDGFRβ image channel), we found no significant change in capillary density (12% larger in subjects depositing Aβ, p=0.56, see Materials and Methods). However, the mean capillary diameter was reduced by 8.1% (p=0.0007) in the patients with Aβ deposition (5121 diameters measured) compared to those without Aβ deposition (3921 diameters measured, Fig. 4C).

To assess whether this diameter reduction was a non-specific effect of AD, or was pericyte-related, we plotted the capillary diameter measurements as a function of the distance from the nearest PDGFRβ-labeled pericyte soma (see Materials and Methods). In patients with no detectable Aβ deposition the capillary diameter increased at locations near pericyte somata compared to at locations far from the somata (~25% larger, slope of line is significantly less than zero, p=3.7×10^{-7} for 813 data points from 6 such patients, Fig. 4D). A similar increase in capillary diameter near somata was previously found in rodent brain capillaries in vivo (19), and attributed to the presence of the soma inducing more growth of the endothelial tube. In contrast, in patients with Aβ deposition, the capillary diameter was significantly reduced near the pericyte somata compared to locations distant from the somata (Fig. 4D; ~30% smaller, slope of line is significantly greater than zero, p=1.6×10^{-20} for 1313 data points from 7 patients), as expected if pericytes cause the capillary constriction by contracting their circumferential processes that are mainly located near their somata. The data shown in Fig. 4D are averaged over all measured pericytes and capillaries (and thus include pericytes on higher branch-order vessels that may be less contractile). For a fixed blood pressure applied at the pial vessels, this average constriction is predicted to reduce flow by ~50% compared to if there were no constriction (see Materials and Methods), which is similar to the 42% decrease observed in the grey matter in patients with AD (3).

The pericyte soma-specific location of the constriction (Fig. 4D) is consistent with the distribution of circumferential processes relative to pericyte somata (Fig. S2) and the fact that exogenous vasoconstrictors constrict capillaries specifically at pericyte locations (Fig. S3; (18)). These data, and the fact that no other cells on capillaries show contractile activity (18), imply that it is pericytes that constrict capillaries in human patients depositing Aβ.

Pericyte constriction of human capillaries increases with Aβ load

The subjects were classified by neuropathologists assessing the Aβ-labeled biopsies as having "no Aβ deposition", "moderate Aβ deposition" or "severe Aβ deposition" in the parenchyma (as diffuse deposits and/or as plaques with central amyloid cores, Fig. 4E). The mean slope for individual patients, from graphs like those in Fig. 4D, for 6 patients with no Aβ deposition, 3 patients with moderate deposition and 4 patients with severe Aβ deposition, showed a progressive change from negative (implying a larger capillary diameter at the soma) to positive (implying a smaller diameter at the soma) as the severity of the Aβ deposition increased (Fig. 4F, p=0.003 compared with a relationship with zero slope). This further supports the idea that Aβ is the cause of the capillary constriction.

To quantify Aβ levels more rigorously, we measured light absorption by the peroxidase product generated by the Aβ antibody, in the region where the vessel diameters were measured in each biopsy (see Materials and Methods; although this measure of Aβ may largely reflect the presence of plaques, it is likely that the soluble Aβ concentration correlates with plaque load). Plotting the slopes of graphs like those in Fig. 4D, for each biopsy, as a function of the amount of Aβ deposition, again showed a monotonic progression from a negative slope to a positive slope as Aβ deposition increased, but with the change of slope occurring more strongly at low levels of Aβ deposition (Fig. 4G). Similarly, plotting the value of the capillary diameter at the pericyte soma for each biopsy (extrapolated from a straight line fit as in Fig. 4D) as a function of Aβ deposition showed that the diameter was reduced strongly by low levels of Aβ, with smaller increments of constriction as deposition increased (Fig. 4H). This presumably reflects the dose-response curve of Fig. 2D (although it could also reflect increased Aβ production when blood flow is less).

Pericytes constrict capillaries in vivo in AD mice

To confirm that pericytes constrict capillaries in vivo in AD (i.e. that the constriction seen in human biopsy tissue was not an artefact of fixing the tissue), and to provide a possible framework for future testing of drugs to prevent this constriction, we used in vivo two-photon imaging of layers I-IV of the somatosensory cortex (Fig. 5A, B) in a mouse model of AD, in which APP with a humanised Aβ region with 3 AD-related mutations ($App^{NL\text{-}G\text{-}F}$) is knocked in (see Materials and Methods). Comparing 4 homozygous AD mice and 3 wild-type (WT) mice (age range P119-P143, when the AD mice already show plaques: Fig. 5C) revealed that, as in human subjects with and without Aβ deposition, in AD mice the mean capillary diameter was less (Fig. 5D, $p=1.7 \times 10^{-9}$), and the diameter at pericyte somata was more strongly reduced (Fig. 5E, $p=1.6 \times 10^{-17}$). A plot of capillary diameter as a function of distance from pericyte somata showed a dilation at the soma in WT mice, but a constriction in the AD mice (Fig. 5F), relative to the diameter midway between somata (cf. Fig. 4D).

To check whether capillary constriction was present throughout the brain of AD mice, or occurred only where Aβ levels rise, we imaged capillaries in vivo in the cerebellum: an area that is relatively spared of amyloid plaque pathology in humans, and that had no plaques in our AD mice at P120-140 (Fig. S5) suggesting lower levels of Aβ oligomers. In cerebellum, both WT and AD mice (n=3 each) showed a larger capillary diameter near pericyte somata (Fig. 5G, p=0.002), with no evidence for a constriction in the AD mice. Thus, capillary constriction is associated with amyloid β production.

Exogenous Aβ has been reported to constrict isolated penetrating arterioles (12) but, at the endogenous level of Aβ produced in the AD mice, arterioles (and venules) were not constricted (Fig. 5H). This may reflect a different response of pericytes and of arteriolar smooth muscle cells to the endothelin-1 released by Aβ (Fig. S6). The lack of arteriole constriction that we observed in the AD mice (Fig. 5H) suggests that capillary constriction is the cause of the decrease in cerebral blood flow that occurs in early AD (1).

Hypoxia is increased in the AD cortex

Our measured capillary constrictions are predicted to decrease cerebral blood flow significantly in AD (see above and Materials and Methods), as has been observed in human patients and AD mice (1, 17, 21). Consistent with this, hypoxic tissue labeling by pimonidazole (hypoxyprobe) was increased significantly in vivo in the AD mice (Fig. S7).

Reversal of Aβ-evoked capillary constriction

Prevention or reversal of Aβ-evoked capillary constriction and tissue hypoxia could be a promising therapy in early AD. In brain slices, we investigated two strategies to achieve this (Fig. S8), assuming it were possible to target drugs specifically to central nervous system (CNS) capillaries. The first strategy involved combined block of the ROS generator NOX4 (with GKT137831, 0.45 μM, Fig. 2F) and of the downstream constricting ET_A receptor (with BQ-123, 1 μM, Fig 2E). This prevented further constriction evoked by Aβ(p=0.027), but did not reverse the capillary diameter to its baseline value on a 1 hour time scale (Fig. 6A). The second strategy employed C-type natriuretic peptide (CNP), which can reverse ET-mediated effects (36) by blocking Ca^{2+} release from internal stores and activating myosin light chain phosphatase (Fig. S8). Remarkably, CNP (100 nM) reversed the Aβ-evoked capillary constriction (p=0.029, Fig. 6A).

Discussion

Genetic evidence strongly implicates Aβ in triggering neuronal damage and cognitive decline in Alzheimer's disease, yet the first change in AD is a decrease of cerebral blood flow (1). Our data make five contributions to understanding the vascular effects of Aβ and their role in Alzheimer's disease: (1) Aβ constricts human and rodent capillaries by acting on pericytes; (2) the mechanism of this constriction involves ROS generation and ET release; (3) in rapidly fixed biopsies from living human patients with Aβ deposition and cognitive decline, cortical capillaries are constricted by 30% at pericyte locations which is sufficient to produce a major reduction of cerebral blood flow; (4) in vivo, in a rodent model of AD, capillaries are constricted by pericytes; and (5) it is in principle possible to reverse the Aβ-evoked capillary constriction. Together, these data imply that the reduction in cerebral blood flow which occurs early in AD results from Aβ-evoked pericyte-mediated constriction of the cerebral capillary bed (Fig. 6B).

At low nanomolar concentrations, exogenous soluble $Aβ_{1−42}$ oligomers evoke a constriction of human and rat cortical capillaries, which is mediated by pericytes. Capillaries are the site in the cortical vasculature where most of the resistance to flow is located (16), and so may be the major site where Aβ produced within the brain can produce vessel diameter changes that reduce cerebral blood flow. In rodents the capillary constriction was the result of Aβ evoking the generation in pericytes and microglia of reactive oxygen species, which evoked a release of endothelin-1 that acted via ET_A receptors to make pericytes constrict the capillaries. We assume that the ET_A receptors involved are located on the pericytes themselves, since ET raised the $[Ca^{2+}]_i$ in pericytes, but we cannot rule out the possibility that they are on a different cell type. The EC_{50} for the action of $Aβ_{1-42}$, 4.7 nM, is

comparable to the concentration of soluble Aβ found in the human AD brain (6 nM, from Table 1 of ref. (37); it is important to note that this brain concentration is higher than the level found in the CSF, which falls during the development of AD as plaques are formed). Thus, wherever Aβ is produced, or can diffuse, in the AD brain, we would expect all contractile pericytes in that region to constrict capillaries. Indeed, our live human biopsy and in vivo mouse imaging data show that the endogenous level of Aβ reached in AD is sufficient to constrict capillaries. However some ageing humans accumulate Aβ and yet do not develop AD - future work could examine whether, in such people, compensation for the vasoconstricting effects of Aβ develops, such as an upregulation of vasodilatory mechanisms.

Throughout this work pericytes were identified by their morphology (spatially isolated cells located outside capillaries) as confirmed by isolectin B_4 labelling, or by antibody labelling for their characteristic marker PDGFRβ, or by expression of dsRed under the NG2 promoter. Although arterioles (recognised as being surrounded by rings of abutting smooth muscle cells) have also been reported to be constricted by exogenous Aβ (12), in AD mice we found no constriction of arterioles. This may be because, at the endothelin-1 level reached during AD pathology, endothelin constricts capillaries but has opposing dilating and constricting effects on arterioles, mediated by different types of ET receptor, which may approximately cancel out. Further work assessing the level of Aβ reached in the AD mice, and the relative affinity of the constricting ET_A and dilating ET_B receptors, will be needed to test this idea.

Three results demonstrate that the effects of Aβ on pericytes that we have demonstrated are pathologically relevant in AD. First, analysing the diameter of capillaries in biopsies from living human patients with cognitive decline, who either had or lacked Aβ, deposition showed that Alzheimer's pathology leads to capillary constriction specifically at pericytes. Second, the magnitude of the capillary constriction in human dementia patients increased with the severity of Aβ deposition and is predicted to produce a decrease of cerebral blood flow (~50%) similar to the 42% seen in AD patients (3). Capillary constriction by pericytes may explain why some capillaries become occluded by neutrophils in AD (37) but neutrophil-block of 2% of capillaries, as observed, was predicted to reduce blood flow by only 5% (38). Finally, in a mouse model of AD, in vivo imaging showed that cerebral capillaries were constricted at pericyte locations, while arterioles and venules were unaffected.

Both the reduction of basal blood flow produced by Aβ, and a reduction in the blood flow increase normally produced by neuronal activity (39), which may also reflect the constricting action of Aβ on pericytes, will decrease the energy supply to the brain. This in turn increases Aβ production by upregulating β-amyloid converting enzyme (β-secretase 1, BACE1) (13, 14). Consequently, the pericyte-mediated capillary constriction evoked by Aβ may act as an amplifying mechanism in a positive feedback loop (Fig. 6B), increasing the levels of Aβ and downstream hyperphosphorylated tau which ultimately lead to the loss of synapses and neurons.

These data suggest several potential therapeutic approaches for early AD, based on the mechanisms generating pericyte constriction. Aβ-evoked generation of reactive oxygen species by NOX4 in pericytes might be targeted. Indeed, overexpression of SOD1 in APP-overexpressing mice abolishes the lethal effects of the APP overexpression (40, 26). Another approach might be to try to reduce endothelin-1 release (presumably from brain cells expressing endothelin-1 strongly, i.e. endothelial cells, microglia or pericytes (28, 29)) or to block the effects of endothelin-1 on its ET_A receptors on CNS pericytes. In a proof-of-concept experiment, a combination of a NOX4 blocker and an ET_A blocker prevented further Aβ-evoked constriction (and could conceivably reverse the existing constriction given sufficient time) while CNP, which acts via two separate pathways downstream of ET (Fig. S8), was able to reverse the constriction in the maintained presence of Aβ. These therapeutic approaches could be tested by targeting drugs to CNS pericytes in the mouse model of AD which also shows the pericyte-mediated constriction of capillaries. Finally, our scheme (Fig. 6B) prompts the question of what fraction of the damage to synapses and neurons in AD reflects direct actions of Aβ and downstream tau, and what fraction is a consequence of the decrease of energy supply that Aβ produces by constricting capillaries.

Materials and Methods

Human brain slices

The work on fresh living human brain tissue received ethical approval from the National Health Service (REC number 15/NW/0568) and all patients gave informed consent. During neurosurgical operations for tumour treatment, apparently normal cortical tissue that was removed (to gain access to the tumour), which would otherwise have been discarded, was placed in ice cold brain slicing solution containing (mM) 93 N-methyl-D-glucamine (NMDG) chloride, 2.5 KCl, 30 $NaHCO_3$, 10 $MgCl_2$, 1.2 NaH_2PO_4, 25 glucose, 0.5 $CaCl_2$, 20 HEPES, 5 Na ascorbate, 3 Na pyruvate, 1 kynurenic acid (to block glutamate receptors, to prevent excitotoxic damage to neurons during the slicing: the experimental solution lacked kynurenic acid, as described below). This solution was oxygenated by gassing with 95% O_2/5% CO_2, and transported in less than 15 mins to the laboratory. Tissue was cut into 200 μm sections and the slices were incubated at 34°C in the same solution for 10 mins, and then incubated at room temperature until used in experiments in a similar solution (41) with the NMDG-Cl, $MgCl_2$ and $CaCl_2$ replaced by (mM) 92 NaCl, 1 $MgCl_2$ and 2 $CaCl_2$. Each patient's tissue typically generated ~2 brain slices. When sufficient tissue was present, histological examination of the slices using haematoxylin and eosin by neuropathologists was used to assess tumour infiltration into the nominally normal tissue. This revealed that while some slices showed no infiltration by the tumour, others did. Aβ was only applied to slices that showed no tumour infiltration. Pericyte responses to noradrenaline and glutamate as documented in Fig. 1 were observed whether or not there was tumour infiltration.

Rodent brain slices

Experiments used P21 Sprague-Dawley rats or transgenic mice as described below of either sex. All animal procedures were carried out in accordance with EU and UK regulations. Cerebral cortical slices (300 μm thick) were prepared (18) and stored as for human slices.

Extracellular solution

Human and rodent brain slices were superfused at 3-4 ml/min with artificial cerebrospinal fluid (aCSF) solution containing (mM) 124 NaCl, 2.5 KCl, 26 $NaHCO_3$, 1 $MgCl_2$, 1 NaH_2PO_4, 10 glucose, 2 $CaCl_2$, 1 Na-ascorbate. This solution was gassed with 20% O_2/75% N_2/5% CO_2, which produces a physiological level of oxygen in the slice near the capillaries being imaged (19). Mechanism-blocking drugs were superfused for 5-15 mins before applying Aβ or ET.

Imaging capillaries in brain slices

Healthy capillaries (<10 μm in diameter, mean diameter 5.61±0.03 μm (n=299) in rat, and 5.08±0.33 μm (n=12) in human, with no rings of arteriolar smooth muscle around them) were selected as previously described (41), and regions of them were imaged which were in focus in a single image plane over at least 30 μm along the length of a capillary and which exhibited a candidate pericyte with a bump-on-a-log morphology (Figs. 1E, 2A). A CCD camera was used to capture images 100 μm square during superfusion of drugs. Capillary diameter was measured from the resulting movies, by an analyst blinded to the time and identity of drug application, by placing a line across the lumen on magnified images using Metamorph software. In some experiments pericytes were identified prior to imaging by incubating slices for 30 min in 10 μg/ml isolectin B_4 conjugated to Alexa 488 or 568 (ThermoFisher I21411 or 121412), which binds to α-D-galactose residues in the basement membrane generated by pericytes and endothelial cells, and outlines pericytes (41). This also allowed two-photon imaging (using a Zeiss LSM710 microscope, excitation wavelength 800 nm) of the endothelial tube and the pericytes on it (Fig. 2B).

Oligomerising Aβ and assessing the form and concentration of Aβ applied

The method employed to generate oligomeric Aβ preparations was modified from that previously described (42). Synthetic $Aβ_{1-42}$ (Bachem H-1368.1000), $Aβ_{1-40}$ (Bachem H-1194.1000) and scrambled $Aβ_{1-42}$ (Bachem H-7406.1000) were suspended in 1,1,1,3,3,3 hexafluoro-2-propanol (HFIP; 52527, Sigma) at 1 mM, vortexed to obtain a homogenous solution, and aliquoted to microcentrifuge tubes. The HFIP was removed by overnight evaporation and the Aβ was completely lyophilised via a Speed-Vac. The Aβ peptide films were stored desiccated at -80°C until further processed (within 2 weeks). The peptide films were then resuspended at a nominal 5 mM in DMSO, bath-sonicated for 10 min and vortexed for 30 sec. To form Aβ oligomers, this solution was diluted to a nominal 100 μM with phosphate-buffered saline, vortexed for 15-30 sec and incubated at 4°C for 24 h. Immediately before use, the oligomeric preparations were centrifuged at 14,000 g for 10 min at 4°C (to remove any fibrils that might be present) and the supernatants were further diluted to the final experimental concentrations (quantified below) with extracellular solution.

Quantification of Aβ peptide concentration was performed using a Pierce BCA protein assay kit (ThermoFisher 23227), calibrated against a known concentration of bovine serum albumin, taking into account the different chromophoric development of albumin and Aβ peptides by multiplying by a factor of 1.51 (43, 44). This showed that the amount of the molecule remaining as soluble monomers and oligomers (i.e. not undissolved or removed as fibrils) was 28.7±2.9% (n=4) of the nominal concentration added for $Aβ_{1-42}$, 39.9±1.5%

(n=4) for $A\beta_{1-40}$, and 43.6±2.3% (n=3) for scrambled $A\beta_{1-42}$. Concentrations stated in the text have been corrected for these factors, and are given based on the monomeric molecular weight. It was not possible to make pure monomeric preparations of $A\beta_{1-42}$ or $A\beta_{1-40}$.

The Aβ oligomeric preparations were analysed via SDS-PAGE using 10-20% tris-glycine gels (EC61352BOX, Invitrogen). Samples of 50 μg Aβ peptides were added to tris-glycine SDS Sample Buffer (LC2676, Invitrogen). Equal volumes of each sample (10 μl) were loaded onto gels along with SeeBluePlus2 (Invitrogen) pre-stained molecular weight markers, and electrophoretically separated at 100 V. Gels were stained for total protein using a SilverXpress Silver Staining kit (LC6100, Invitrogen) according to the manufacturer's protocol. $A\beta_{1-42}$ and $A\beta_{1-40}$ formed monomers and oligomers, while scrambled $A\beta_{1-42}$ formed mainly monomers (Fig. 1G). Using densitometry we estimated that for Fig. 1G the percentages of $A\beta_{1-42}$, $A\beta_{1-40}$ and scrambled $A\beta_{1-42}$ present as monomers (defined as molecular weight 2.5-6.5 kD) were 48%, 39% and 89% respectively; the percentages as dimers (MW 6.5-11.5 kD) were 11%, 46% and 11%; the percentages as trimers (MW 11.5-15.5 kD) were 22%, 6% and 0%; and the percentages as tetramers (MW 15.5-20.5 kD) were 19%, 4% and 0%. Thus, the measured EC_{50} of 4.7 nM for the effect of $A\beta_{1-42}$ on constriction in Fig. 1D, which was calculated based on the monomeric molecular weight, would become approximately 4.7x0.19 = 0.9 nM if only the tetramer was active.

Immunohistochemistry of non-biopsy tissue

Human and rat brain slices were fixed in 4% paraformaldehyde (PFA) for 1 hour, washed 3 times in phosphate-buffered saline (PBS), then blocked in 10% goat serum/0.5% Triton X100 in PBS. Primary antibodies for PDGFRβ (Santa Cruz, sc432, 1:200) or α-SMA (Santa Cruz, CGA7, 1:200) or Aβ (IBL, 82E1, 1:500) were applied overnight, followed (after washing in PBS) by application overnight of Alexa Fluor 647 or 633 conjugated secondary antibodies (ThermoFisher, A-21245, A-21070, A-21050, 2 μg/ml). Slices were then washed once in PBS containing DAPI nuclear stain (1:50,000) for 10 mins and then washed again in PBS. After mounting, slices were imaged on a Zeiss LSM700 confocal microscope.

Imaging pericyte $[Ca^{2+}]_i$

Experiments were carried out on acute cortical brain slices from P44-P88 mice, of either sex, generated by crossing tamoxifen-inducible NG2-Cre^{ERT2} mice (45) with floxed GCaMP5G-IRES-tdTomato mice (JAX 024477). Co-expression of the genetically encoded Ca^{2+} indicator GCaMP5G and the morphological marker tdTomato (driven by the CAG promoter after Cre-mediated recombination) was induced by oral gavage of tamoxifen (1 mg/10 g bodyweight) for four consecutive days (starting from P23). Brain slices (300 μm thick) were prepared from 21 days after the first tamoxifen administration, as described above for human and rat brain slices. Cortical capillary pericytes, identified in the tdTomato channel from their bump-on-a-log somatic morphology and processes wrapped around capillaries, were imaged using a two-photon microscope (Zeiss LSM 710 or 780) with the two-photon laser (Ti:sapphire Mai Tai DeepSee, Spectra Physics) tuned to 940 nm. Images were acquired with a 20x/1.0 NA water immersion objective (W Plan-Apochromat, Zeiss). Laser power was 5-20 mW in the focal plane. Emitted fluorescence was spectrally divided by a 555 nm dichroic mirror, and collected by GaAsP detectors. Two-photon image stacks (50-200 μm x

50-200 μm x 20-40 μm, 150-300 nm pixel size, 2 μm z-step size, 1.58-2.55 μs pixel dwell time) were acquired every 30 seconds, and processed using FIJI (ImageJ). Image-stacks were first maximum intensity projected in the z-dimension, and both channels were co-registered to correct for movement artefacts using the FIJI plugin Multistackreg. Percentage changes in the GCaMP5G fluorescence of regions of interest (ROIs) drawn around pericyte somata were calculated. Oligodendrocyte precursor cells (OPCs), identified based on a star-like morphology and weaker baseline fluorescence, and arteriolar smooth muscle cells, were excluded from the analysis.

Assessing pericyte death

This was carried out as previously described (19). Briefly, brain slices (250 μm thick) were incubated at $36\pm1°C$ in a multi-well plate, with 95% O_2/5% CO_2 blown gently at the surface, in aCSF, or aCSF with oligomerised $A\beta_{1-42}$ or ET added. All extracellular solutions contained isolectin B_4 (41) to label the basement membrane (ThermoFisher I21411, 10 μg/ml), and hence to label pericytes which are enveloped by this (Fig. 1B), and 7.5 μM propidium iodide to label cells with membranes that had become non-specifically permeable (19). After 3 hours incubation, slices were fixed in 4% PFA for 2 hours, washed 3 times with PBS for 15 mins each, mounted in DAKO medium and imaged on a confocal microscope. To avoid counting cells killed by the slicing procedure, quantification of the percentage of pericytes that were dead excluded cells within 20 μm of the slice surface.

Imaging ROS production

Cellular production of reactive oxygen species (ROS) in brain slices was visualised through the $O_2^{\cdot-}$-specific oxidation of dihydroethidium to ethidium, which binds to the DNA and RNA of $O_2^{\cdot-}$-producing cells (46). Rat cortical slices (250 μm thick) were incubated in aCSF or in aCSF containing $A\beta_{1-42}$ (72 nM) or $A\beta_{1-42}$ + SOD1 (150 units/ml) at 34°C. Dihydroethidium (DHE, 8 μM, Cayman, 104821) was added to all solutions immediately before use to avoid auto-oxidation of the dye. No preincubation with DHE was used, to limit the intracellular accumulation of oxidised product. After 40 min, the slices were quickly rinsed in PBS, mounted and immediately imaged using a confocal microscope. A single image stack was acquired at the middle of each slice and for Fig. 3B the fluorescence intensity of the maximum intensity projections was measured using ImageJ. For establishing the identity of ROS-producing cells, slices were fixed in 4% PFA for 20 min and immunostained for NG2 (Millipore AB5320, 1:200) and Iba1 (Synaptic Systems 234006, 1:200). Alexa 488-isolectin B_4 (ThermoFisher I21411, 10 μg/ml) was added with the secondary antibodies to also label blood vessels. In maximum intensity projections of z-stacks, ROIs were then drawn around the nuclei of pericytes (NG2-expressing cells on capillaries) and Iba1-expressing immune cells (microglia and perivascular macrophages) and the DHE signal within each ROI was measured in ImageJ. For each z-stack, a mean intensity per pericyte or Iba-1-labeled cell, and the total intensity per population of pericytes or Iba1-labeled cells, were calculated, and analysis was performed using the z-stack as the statistical unit.

For glutathione imaging, rat brain slices were incubated with Aβ and fixed as described above, then incubated with 10 mM N-ethylmaleimide (NEM) for 4 h at 4°C and washed

thoroughly with PBS. The sections were additionally immunolabeled with a GSH-NEM antibody (Millipore MAB3194, 1:500) which is specific to this adduct, allowing quantification of reduced glutathione after reaction with NEM (47). Following confocal imaging, ROIs were drawn around the soma of IB$_4$-labeled pericytes and Iba1-expressing immune cells as above and the total fluorescence signal for GSH-NEM was quantified for each cell and averaged over cells.

Human biopsy data

Diagnostic brain biopsies, comprising cortex and subcortical white matter, were performed as part of routine clinical investigation at the National Hospital for Neurology and Neurosurgery, Queen Square, London, to exclude treatable causes of neurological symptoms that patients showing cognitive decline had presented with. All patients gave informed consent for the biopsy. The use of human tissue samples was licensed by the National Research Ethical Service, UK (University College London Hospitals NRES license for using human tissue samples, project ref 08/0077). The storage of human tissue was licensed by the Human Tissue Authority, UK (License #12054).

Biopsies (volume typically 1 cm^3) were all from the right frontal lobe. The biopsies were fixed in 10% buffered formalin less than 30 mins after the resection, for a minimum of 12 hours. The formalin-fixed tissue was dehydrated through graded alcohols and embedded in paraffin wax, from which 4 μm thick sections were cut for routine haematoxylin and eosin staining and a panel of immunohistochemical stains. As part of the diagnostic work up, the sections were immunostained for Aβ with immunoperoxidase-labeled antibody 6F3D (DAKO, 1:50), and for this study in addition with antibody against PDGFRβ (RD systems, MAB1263, 1:20) to label pericytes. This was performed on a Roche Ventana Discovery automated staining platform following the manufacturer's guidelines, using biotinylated secondary antibodies and streptavidin-conjugated horseradish peroxidase and diaminobenzidine as the chromogen. The extent of parenchymal Aβ deposition was assessed semi-quantitatively as absent, moderate or severe by a neuropathologist. In addition, to objectively quantify Aβ deposition, the images of the immunoperoxidase label for Aβ were imported into ImageJ, and split into red, green and blue channels. Then, the light intensity in the blue channel (which gave best distinction of the immunoperoxidase label from the background tissue haematoxylin labeling) was measured in the region of the biopsy where diameters were measured, normalised by the intensity in a region of the section showing no visible Aβ label and converted to a percentage of light absorbed by the Aβ. Normalising by the intensity in a (tissue-free) region without any tissue absorption gave values that were 5.8±0.5% larger, which did not materially change the form of the graphs. Although this measure of Aβ may largely reflect the presence of plaques, it is likely that the soluble Aβ concentration correlates with plaque load (48).

The mean age of patients without Aβ deposition was 50.5±5.5 (n=6, 4 women and 2 men), and of those with Aβ deposition was 62.1±4.2 (n=7, 4 women and 3 men, not significantly different, p=0.11). Regressing mean capillary diameter against age from all patients, or from the patients lacking Aβ deposition, showed that there was no significant dependence on age (p=0.5 and p=0.82 respectively).

Images were analysed to assess capillary diameter with the experimenter blinded to the level of Aβ deposits (i.e. viewing only the PDGFRβ channel: the condition of the tissue was sometimes worse for patients with Aβ deposition, but it was not possible to unambiguously decide whether the patient had Aβ deposition without viewing the Aβ channel). A standard 5x4 grid of 20 squares (each with sides 400 μm long) was superimposed on each image, and all capillaries with clearly demarcated endothelial walls visible in each square had their diameter measured. The image squares were treated as the experimental unit for statistical analysis. Analysis of the diameter as a function of distance from the nearest visible pericyte employed a subset of all the measured diameters, because often no pericyte was visible on some short capillary segments. The total number of measurable capillary segments (within the 5x4 grid) per subject was not significantly different (p=0.56) between subjects depositing Aβ (732±96) and subjects not depositing Aβ (654±88), suggesting no detectably greater loss of capillaries in the subjects depositing Aβ.

Experiments in vivo on AD mice

AD mice, in which APP with a humanised Aβ region containing 3 AD-related mutations (APP^{NL-G-F}) is knocked in (49), to avoid artefacts associated with over-expressing APP, were crossed with NG2-DsRed mice in which pericytes express DsRed (19). Mice aged ~4 months (P119-P143, not significantly different for WT and AD, p=0.13) were anesthetised using urethane (1.55 g/kg given in two doses 15 minutes apart). Adequate anesthesia was ensured by confirming the absence of a withdrawal response to a paw pinch. Body temperature was maintained at 36.8±0.3°C and eyes were protected from drying by applying polyacrylic acid eye drops (Dr. Winzer Pharma). The animal was secured in a stereotaxic frame and lidocaine/prilocaine (AstraZeneca) was applied topically prior to exposing the skull. A custom built headplate was then attached to the skull using superglue to create a sealed well filled with HEPES-buffered aCSF (in mM: 140 NaCl, 10 HEPES, 2.5 KCl, 1 NaH_2PO_4, 10 glucose, 2 $CaCl_2$, 1 $MgCl_2$) during imaging. A craniotomy of approximately 3 mm diameter was performed over the right primary somatosensory cortex, immediately caudal to the coronal suture and approximately 2-6 mm laterally from the midline, or over the right cerebellar hemisphere for imaging cerebellar vessels. The dura was left intact, to reduce perturbation of the brain. During imaging, the headplate was secured under the objective on a custom built stage.

Cortical or cerebellar vessel diameter was recorded using two-photon microscopy of the intraluminal dyes Cascade Blue dextran (MW 10 kDa, Invitrogen, D1976, 1.25 mg in 100 μl saline given i.v.) or albumin–fluorescein isothiocyanate conjugate (FITC-albumin, Sigma, A9771, 1 mg in 100 μl saline given retro-orbitally). Two-photon excitation was carried out using a Newport-Spectraphysics Ti:Sapphire MaiTai laser pulsing at 80 MHz, and a Zeiss LSM710 microscope with a 20x water immersion objective (NA 1.0). Fluorescence was evoked using a wavelength of 920 nm for DsRed, 820 nm for FITC-albumin and 800 nm for Cascade-Blue. The mean laser power under the objective did not exceed 35 mW. Penetrating arterioles >10 μm in size were identified by the typical ring shape of vascular smooth muscle cells expressing DsRed in NG2-DsRed (wild-type or APP^{NL-G-F}) mice. Image stacks were taken in 2 μm depth increments across layers I-IV of the cortex (up to 400 μm deep from the cortical surface). To measure vessel diameter, a line was drawn in ImageJ across the vessel

perpendicular to its axis and the width of the intraluminal dye fluorescence was measured, either manually or using an automated routine fitting a Gaussian function to the fluorescence profile in ImageJ and calculating the full width at quarter-maximum of the peak fluorescence intensity (which gave results insignificantly different from the manual measurement).

Assessing hypoxia in vivo with pimonidazole

Hypoxia was assessed in vivo using the Hypoxyprobe-Plus (HP2-100, Hypoxyprobe Inc.) kit following the manufacturer's instructions. Following anesthesia induction with 3% isoflurane in air, animals were switched to 1.5% isoflurane in air and 60 mg/kg pimonidazole HCl was injected intraperitoneally. Four hours after pimonidazole injection, animals were transferred to 1.55g/kg urethane anesthesia and sacrificed by perfusion fixation. Brains were extracted and kept in paraformaldehyde for 24 hours prior to sectioning for immuno-histochemistry using the FITC-conjugated antibody provided in the kit which recognises conjugates of pimonidazole with protein SH groups in hypoxic cells.

Statistics

Data are presented as mean±s.e.m. Data normality was assessed with Shapiro-Wilk or D'Agostino-Pearson omnibus tests. Comparisons of normally distributed data were made using 2-tailed Student's t-tests. Equality of variance was assessed with an F test, and heteroscedastic t-tests were used if needed. Data that were not normally distributed were analysed with Mann-Whitney tests. P values were corrected for multiple comparisons using a procedure equivalent to the Holm-Bonferroni method (for N comparisons, the most significant p value is multiplied by N, the 2nd most significant by N-1, the 3rd most significant by N-2, etc.; corrected p values are significant if they are less than 0.05). Assessment of whether the slope of linear regressions differed significantly from zero was obtained using the t-statistic for the slope. P values comparing vessel diameters in the absence and presence of drugs were calculated for the last data point in each graph shown, or for an exposure time of 45-60 mins if no graph is shown. An estimate of the sample size needed for a typical experiment is as follows: For a control response of 100%, a response standard deviation of 10%, a response in a drug of 70% (30% inhibition), a power of 80% and p<0.05, less than 6 vessels are needed in each of the control and drug groups (www.biomath.info/power/ttest.htm). The exact numbers depend on the drug effect size and standard error of the data.

Calculation of effect of vessel constriction on flow

We assume that pericytes are regularly spaced on capillaries at an interval of 2L. For flow governed by Poiseuille's law, the resistance of a segment of capillary of length L (from a pericyte soma to midway between two pericytes) and radius r_1 is given by

$$k \cdot L/r_1^4$$

where k is a constant. If Aβ-induced pericyte contraction reduces the capillary diameter from a value of r_1 at the midpoint between pericytes to r_2 near the pericyte soma (see Fig.

4A, B, D), then if this reduction is linear with distance the resistance of the capillary segment from the soma to the midpoint is given by

$$k \cdot L \cdot (r_1{}^2 + r_1 \cdot r_2 + r_2{}^2)/(3 \cdot r_1{}^3 r_2{}^3)$$

so the factor by which the resistance is altered (compared to that with a uniform diameter r_1) is

$$[1 + (r_1/r_2) + (r_1/r_2)^2] \cdot (r_1/r_2)/3 \quad (1)$$

Thus, with Aβ deposition, the 30% pericyte constriction reported at pericyte somata in Fig. 4D will increase the resistance by a factor of 2.1, compared to a situation with the capillary having a uniform diameter equal to that measured far from the pericyte somata (~3.9 μm in Fig. 4D), while the 27% increase in diameter at the soma in subjects without Aβ deposition will decrease the resistance to 0.63 of the value with a uniform capillary. Taking the ratio of these changes leads to the conclusion that the capillary constriction occurring with Aβ deposition will increase the capillary resistance by a factor of 3.4 (compared to the condition with no Aβ deposition). Since the capillaries provide 57% of the total vascular resistance in the brain parenchyma (16), and the diameter of arterioles and venules is not changed (Fig. 5H), it follows that, if the pressure is fixed at the pial end of penetrating arterioles and venules, then cerebral blood flow will be decreased by 58% (calculated as (43%+57%)/(43% +3.4x57%)). In reality the flow reduction could be greater than this because Poiseuille's law does not apply for small capillary diameters for which the effective blood viscosity increases as the diameter decreases below 10 μm (50). Importantly, the data in Fig. 4 were averaged over all visible pericytes in the images, and so already take account of the fact that the contractility of capillary pericytes decreases for higher branching orders of capillary (19).

Supplementary Material

Refer to Web version on PubMed Central for supplementary material.

Acknowledgements

Nortley et al. Page 18

References

1. Iturria-Medina Y, Sotero RC, Toussaint PJ, Mateos-Pérez JM, Evans AC. Alzheimer's Disease Neuroimaging Initiative, Early role of vascular dysregulation on late-onset Alzheimer's disease based on multifactorial data-driven analysis. Nat Comm. 2016; 7

2. Love S, Miners JS. Cerebrovascular disease in ageing and Alzheimer's disease. Acta Neuropathol. 2016; 131:645–658. [PubMed: 26711459]

3. Asllani I, Habeck C, Scarmeas N, Borogovac A, Brown TR, Stern Y. Multivariate and univariate analysis of continuous arterial spin labeling perfusion MRI in Alzheimer's disease. J Cereb Blood Flow Metab. 2008; 28:725–736. [PubMed: 17960142]

4. Kang J, Lemaire HG, Unterbeck A, Salbaum JM, Masters CL, Grzeschik KH, Multhaup G, Beyreuther K, Müller-Hill B. The precursor of Alzheimer's disease amyloid A4 protein resembles a cell-surface receptor. Nature. 1987; 325:733–736. [PubMed: 2881207]

5. Hardy, Allsop D. Amyloid deposition as the central event in the aetiology of Alzheimer's disease. Trends Pharmacol Sci. 1991; 12:383–388. [PubMed: 1763432]

6. Selkoe DJ. The molecular pathology of Alzheimer's disease. Neuron. 1991; 6:487–498. [PubMed: 1673054]

7. Kimura T, Hashimura T, Miyakawa T. Observations of microvessels in the brain with Alzheimer's disease by the scanning electron microscope. Jap J Psychiatr Neurol. 1991; 45:671–676.

8. de la Torre JC, Mussivand T. Can disturbed brain microcirculation cause Alzheimer's disease? Neurol Res. 1993; 15:146–153. [PubMed: 8103579]

9. Thomas T, Thomas G, McLendon C, Sutton T, Mullan M. β-Amyloid-mediated vasoactivity and vascular endothelial damage. Nature. 1996; 380:168–171. [PubMed: 8600393]

10. Suo Z, Humphrey J, Kundtz A, Sethi F, Placzek A, Crawford F, Mullan M. Soluble Alzheimer's β-amyloid constricts the cerebral vasculature in vivo. Neurosci Lett. 1998; 257:77–80. [PubMed: 9865931]

11. Deane R, Du Yan S, Submamaryan RK, LaRue B, Jovanovic S, Hogg E, Welch D, Manness L, Lin C, Yu J, Zhu H, et al. RAGE mediates amyloid-beta peptide transport across the blood-brain barrier and accumulation in brain. Nat Med. 2003; 9:907–913. [PubMed: 12808450]

12. Dietrich HH, Xiang C, Han BH, Zipfel GJ, Holtzman DM. Soluble amyloid-beta, effect on cerebral arteriolar regulation and vascular cells. Molec Neurodegen. 2010; 5:15.

13. Sun X, He G, Qing H, Zhou W, Dobie F, Cai F, Staufenbiel M, Huang LE, Song W. Hypoxia facilitates Alzheimer's disease pathogenesis by up-regulating BACE1 gene expression. Proc Natl Acad Sci USA. 2006; 103:18727–18732. [PubMed: 17121991]

14. Zhang X, Zhou K, Wang R, Cui J, Lipton SA, Liao FF, Xu H, Zhang YW. Hypoxia-inducible factor 1α(HIF-1α)-mediated hypoxia increases BACE1 expression and β-amyloid generation. J Biol Chem. 2007; 282:10873–10880. [PubMed: 17303576]

15. Niwa K, Porter VA, Kazama K, Cornfield D, Carlson GA, Iadecola C. Aβ-peptides enhance vasoconstriction in cerebral circulation. Am J Physiol Heart Circ Physiol. 2001; 281:H2417–2424. [PubMed: 11709407]

16. Gould IG, Tsai P, Kleinfeld D, Linninger A. The capillary bed offers the largest hemodynamic resistance to the cortical blood supply. J Cereb Blood Flow Metab. 2017; 37:52–68. [PubMed: 27780904]

17. Nielsen RB, Egefjord L, Angleys H, Mouridsen K, Gejl M, Møller A, Brock B, Brændgaard H, Gottrup H, Rungby J, Eskildsen SF, et al. Capillary dysfunction is associated with symptom severity and neurodegeneration in Alzheimer's disease. Alz Dement. 2017; 13:1143–1153.

18. Peppiatt CM, Howarth C, Mobbs PG, Attwell D. Bidirectional control of CNS capillary diameter by pericytes. Nature. 2006; 443:700–704. [PubMed: 17036005]

19. Hall CN, Reynell C, Gesslein B, Hamilton NB, Mishra A, Sutherland BA, O'Farrell FM, Buchan AM, Lauritzen M, Attwell D. Capillary pericytes regulate cerebral blood flow in health and disease. Nature. 2014; 508:55–60. [PubMed: 24670647]

20. Attwell D, Mishra A, Hall CN, O'Farrell FM, Dalkara T. What is a pericyte? J Cereb Blood Flow Metab. 2016; 36:451–455. [PubMed: 26661200]

21. Gutiérrez-Jiménez E, Angleys H, Rasmussen PM, West MJ, Catalini L, Iversen NK, Jensen MS, Frische S, Østergaard L. Disturbances in the control of capillary flow in an aged APPswe/PS1 E9 model of Alzheimer's disease. Neurobiol Aging. 2017; 62:82–94. [PubMed: 29131981]

22. Klein WL, Krafft GA, Finch CE. Targeting small Aβ oligomers: the solution to an Alzheimer's disease conundrum? Trends Neurosci. 2001; 24:219–224. [PubMed: 11250006]

23. Attems J, Lintner F, Jellinger KA. Amyloid β peptide 1-42 highly correlates with capillary cerebral amyloid angiopathy and Alzheimer disease pathology. Acta Neuropathol. 2004; 107:283–291. [PubMed: 14986026]

24. Alarcon-Martinez L, Yilmaz-Ozcan S, Yemisci M, Schallek J, Kılıç K, Can A, Di Polo A, Dalkara T. Capillary pericytes express α-smooth muscle actin, which requires prevention of filamentous-actin depolymerization for detection. Elife. 2018; 7:e34861. [PubMed: 29561727]

25. Love S, Palmer J. Endothelin receptor antagonists: potential in Alzheimer's disease. Pharmacol Res. 2011; 63:525–531. [PubMed: 21193044]

26. Iadecola C, Zhang F, Niwa K, Eckman C, Turner SK, Fischer E, Younkin S, Borchelt DR, Hsiao KK, Carlson GA. SOD1 rescues cerebral endothelial dysfunction in mice overexpressing amyloid precursor protein. Nat Neurosci. 1999; 2:157–161. [PubMed: 10195200]

27. Kuroda J, Ago T, Nishimura A, Nakamura K, Matsuo R, Wakisaka Y, Kamouchi M, Kitazono T. Nox4 is a major source of superoxide production in human brain pericytes. J Vasc Res. 2014; 51:429–438. [PubMed: 25612841]

28. Zhang Y, Chen K, Sloan SA, Bennett ML, Scholze AR, O'Keeffe S, Phatnani HP, Guarnieri P, Caneda C, Ruderisch N, Deng S, et al. An RNA-Seq transcriptome and splicing database of glia, neurons, and vascular cells of the cerebral cortex. J Neurosci. 2014; 34:11929–11947. [PubMed: 25186741]

29. Zeisel A, Hochgerner H, Lönnerberg P, Johnsson A, Memic F, van der Zwan J, Häring M, Braun E, Borm LE, La Manno G, Codeluppi S, et al. Molecular architecture of the mouse nervous system. Cell. 2018; 174:999–1014. [PubMed: 30096314]

30. Luo J, Grammas P. Endothelin-1 is elevated in Alzheimer's disease brain microvessels and is neuroprotective. J Alzheimers Dis. 2010; 21:887–896. [PubMed: 20634595]

31. Palmer JC, Barker R, Kehoe PG, Love S. Endothelin-1 is elevated in Alzheimer's disease and upregulated by amyloid-β. J Alzheimers Dis. 2012; 29:853–861. [PubMed: 22330820]

32. Paris D, Humphrey J, Quadros A, Patel N, Crescentini R, Crawford F, Mullan M. Vasoactive effects of Aβ in isolated human cerebrovessels and in a transgenic mouse model of Alzheimer's disease: role of inflammation. Neurol Res. 2003; 25:642–651. [PubMed: 14503019]

33. Hamilton NB, Attwell D, Hall CN. Pericyte-mediated regulation of capillary diameter: a component of neurovascular coupling in health and disease. Front Neuroenergetics. 2010; 2:5. [PubMed: 20725515]

34. Bianca VD, Dusi S, Bianchini E, Dal Prà I, Rossi F. β-amyloid activates the $O_2^\cdot$ forming NADPH oxidase in microglia, monocytes, and neutrophils. A possible inflammatory mechanism of neuronal damage in Alzheimer's disease. J Biol Chem. 1999; 274:15493–15499. [PubMed: 10336441]

35. Park L, Uekawa K, Garcia-Bonilla L, Koizumi K, Murphy M, Pistik R, Younkin L, Younkin S, Zhou P, Carlson G, Anrather J, et al. Brain perivascular macrophages initiate the neurovascular dysfunction of Alzheimer Aβ peptides. Circ Res. 2017; 121:258–269. [PubMed: 28515043]

36. Špiranec K, Chen W, Werner F, Nikolaev VO, Naruke T, Koch F, Werner A, Eder-Negrin P, Diéguez-Hurtado R, Adams RH, Baba HA, et al. Endothelial C-type natriuretic peptide acts on pericytes to regulate microcirculatory flow and blood pressure. Circulation. 2018; 138:494–508. [PubMed: 29626067]

37. Roberts BR, Lind M, Wagen AZ, Rembach A, Frugier T, Li QX, Ryan TM, McLean CA, Doecke JD, Rowe CC, Villemagne VL, et al. Biochemically-defined pools of amyloid-β in sporadic Alzheimer's disease: correlation with amyloid PET. Brain. 2017; 140:1486–1498. [PubMed: 28383676]

38. Cruz Hernández JC, Bracko O, Kersbergen CJ, Muse V, Haft-Javaherian M, Berg M, Park L, Vinarcsik LK, Ivasyk I, Rivera DA, Kang Y, et al. Neutrophil adhesion in brain capillaries reduces

cortical blood flow and impairs memory function in Alzheimer's disease mouse models. Nat Neurosci. 2019; 22:413–420. [PubMed: 30742116]

39. Park L, Anrather J, Forster C, Kazama K, Carlson GA, Iadecola C. Abeta-induced vascular oxidative stress and attenuation of functional hyperemia in mouse somatosensory cortex. J Cereb Blood Flow Metab. 2004; 24:334–342. [PubMed: 15091114]

40. Carlson GA, Borchelt DR, Dake A, Turner S, Danielson V, Coffin JD, Eckman C, Meiners J, Nilsen SP, Younkin SG, Hsiao KK. Genetic modification of the phenotypes produced by amyloid precursor protein overexpression in transgenic mice. Hum Mol Genet. 1997; 6:1951–1959. [PubMed: 9302276]

41. Mishra A, O'Farrell FM, Reynall C, Hamilton NB, Hall CN, Attwell D. Imaging pericytes and capillary diameter in brain slices and isolated retinae. Nat Protoc. 2014; 9:323–336. [PubMed: 24434801]

42. Lambert MP, Viola KL, Chromy BA, Chang L, Morgan TE, Yu J, Venton DL, Krafft GA, Finch CE, Klein WL. Vaccination with soluble Aβ oligomers generates toxicity-neutralizing antibodies. J Neurochem. 2001; 79:595–605. [PubMed: 11701763]

43. Jan A, Hartley DM, Lashuel HA. Preparation and characterization of toxic Aβ aggregates for structural and functional studies in Alzheimer's disease research. Nat Prot. 2010; 5:1186–1209.

44. www.amidebio.com/wp-content/uploads/2016/07/Abeta_Quantitation_Protocol.pdf

45. Huang W, Zhao N, Bai X, Karram K, Trotter J, Goebbels S, Scheller A, Kirchhoff F. Novel NG2-CreERT2 knock-in mice demonstrate heterogeneous differentiation potential of NG2 glia during development. Glia. 2014; 62:896–913. [PubMed: 24578301]

46. Wu L-J, Wu G, Akhavan Sharif MR, Baker A, Jia Y, Fahey FH, Luo HR, Feener EP, Clapham DE. The voltage-gated proton channel, Hv1, enhances brain damage from ischemic stroke. Nat Neurosci. 2012; 15:565–573. [PubMed: 22388960]

47. Won SJ, Kim JE, Cittolin-Santos GF, Swanson RA. Assessment at the single-cell level identifies neuronal glutathione depletion as both a cause and effect of ischemia-reperfusion oxidative stress. J Neurosci. 2015; 35:7143–7152. [PubMed: 25948264]

48. Murphy MP, Levine H III. Alzheimer's disease and the β-amyloid peptide. J Alzheimer's Dis. 2010; 19:311–323. [PubMed: 20061647]

49. Saito T, Matsuba Y, Mihira N, Takano J, Nilsson P, Itohara S, Iwata N, Saido TC. Single *App* knock-in mouse models of Alzheimer's disease. Nat Neurosci. 2014; 1:661–663.

50. Pries AR, Secomb TW, Gaehtgens P, Gross JF. Blood flow in microvascular networks. Experiments and simulation. Circ Res. 1990; 67:826–834. [PubMed: 2208609]

51. Arteel GE, Thurman RG, Yates JM, Raleigh JA. Evidence that hypoxia markers detect oxygen gradients in liver: pimonidazole and retrograde perfusion of rat liver. Brit J Cancer. 1995; 72:889–895. [PubMed: 7547236]

52. Buzsáki G, Kaila K, Raichle M. Inhibition and brain work. Neuron. 2006; 56:771–783.

One sentence summary

Amyloid β acts on pericytes to reduce brain energy supply in humans with cognitive decline

Print page summary

Introduction

Alzheimer's disease (AD) and other dementias are an increasing socio-economic burden as the population lives to reach older ages. In AD, the production of amyloid β (Aβ) oligomers and downstream tau dysfunction are thought to cause neuronal damage, in particular a loss of synapses and synaptic plasticity, which results in cognitive impairment. However, epidemiological data show that vascular factors are important contributors to AD risk, and biomarker research has shown that the first change in AD is a decrease of cerebral blood flow. Because most of the vascular resistance within the brain is located in capillaries, this could reflect a dysfunction of contractile pericytes on capillary walls. Indeed, pericytes are known to regulate cerebral blood flow physiologically and to severely restrict blood flow after stroke.

Rationale

We examined the role of pericytes in Alzheimer's disease by examining cerebral capillaries in humans and mice developing AD, and by applying Aβ to capillaries. We used freshly fixed brain biopsies from cognitively impaired living humans who were depositing Aβ plaques, and carried out in vivo imaging in a knock-in mouse model of AD. We measured capillary diameters at positions near pericytes, in order to assess whether the capillaries became constricted in AD, because this would lead to a decrease of cerebral blood flow and hence a decrease of the glucose and oxygen supply to the brain tissue. In addition, to investigate one mediator already thought to be important in AD, we applied Aβ to human brain slices made from normal tissue that was removed from patients undergoing neurosurgical glioma resection, and to rodent brain slices. Aβ was applied in the oligomeric form, which is thought to contribute to cognitive decline. This allowed us to examine whether Aβ itself might alter cerebral blood flow, and to use pharmacology to investigate the mechanism of any such effect.

Results

Both in humans developing AD and in the mouse model of AD, capillaries were constricted specifically at pericyte locations, but arterioles and venules were unchanged in diameter. Thus, the reduction of cerebral blood flow known to occur in AD is produced by capillaries, rather than arterioles. The capillary constriction increased rapidly with the severity of Aβ deposition, and was calculated to become sufficient in human cortex to approximately halve cerebral blood flow, which is comparable to the decrease of blood flow measured experimentally in affected parts of the AD brain. In the AD mouse cerebellum, which lacks Aβ deposition at the age examined, there was no capillary constriction, supporting the idea of a causal link between Aβ level and constriction of capillaries. Aβ itself was found to constrict both human and rodent capillaries, by a mechanism involving the generation of reactive oxygen species, mainly by NADPH oxidase 4 (NOX4). The reactive oxygen species then triggered the release of endothelin-1, which acted on ET_A receptors to evoke pericyte contraction, thus causing capillary constriction. The Aβ-evoked constriction could be halted by blocking NOX4

and ET$_A$ receptors, and was reversed by applying the vasodilator C-type natriuretic peptide.

Conclusion

These data reconcile genetic evidence for a role of Aβ in triggering neuronal damage and cognitive decline in AD with the first clinically-detectable change in AD being a decrease of cerebral blood flow. They imply that attention should be given to vascular mechanisms in AD as well as to signaling pathways that act directly on neurons or glia, and suggest novel therapeutic approaches for treating early AD by targeting drugs to brain pericytes. They also raise the question of what fraction of the damage to synapses and neurons in AD reflects direct actions of Aβ and downstream tau, and what fraction is a consequence of the decrease of energy supply that Aβ produces by constricting capillaries.
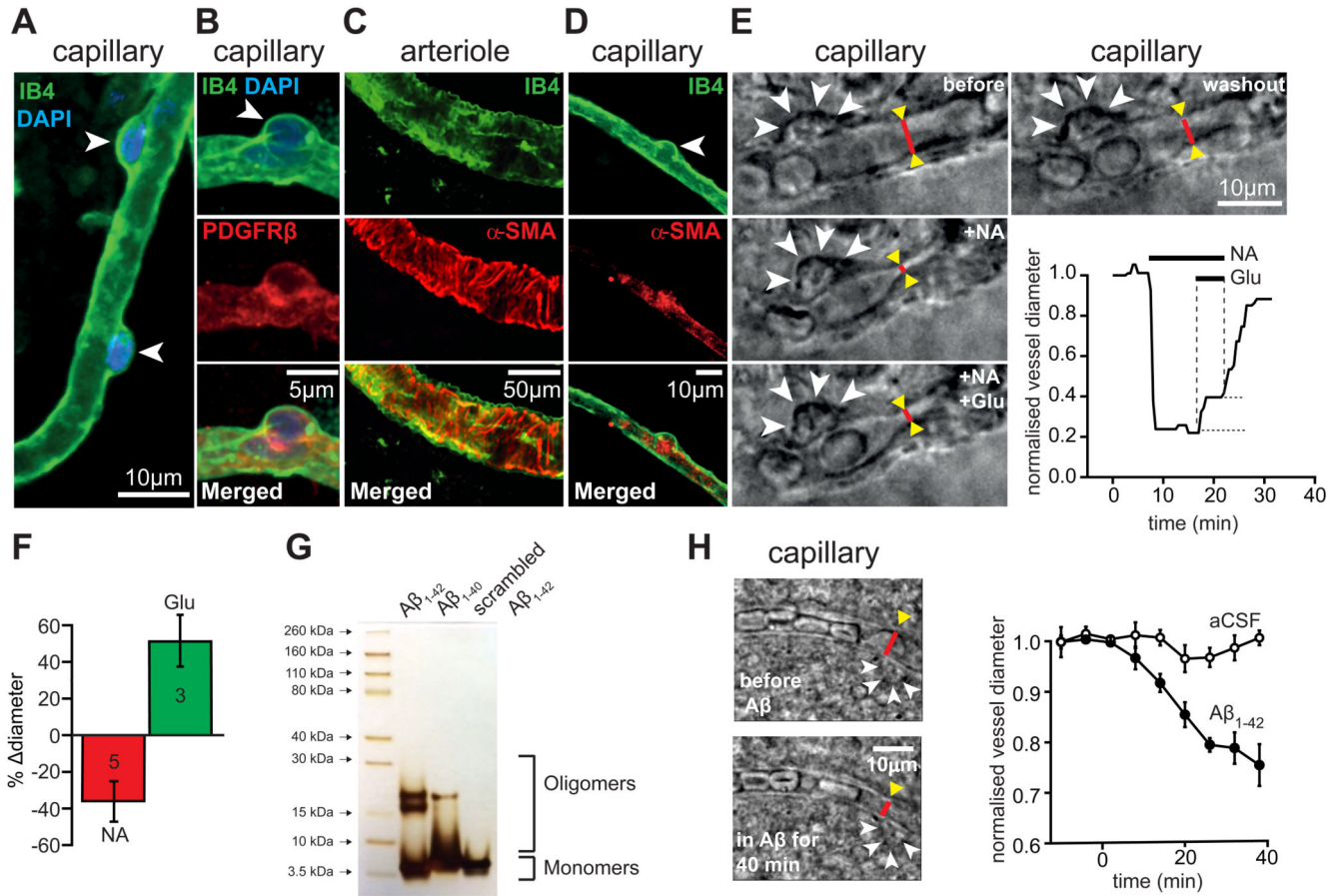
Figure 1. Oligomeric Aβ acts on pericytes to constrict capillaries in human brain slices.
(**A**) Isolectin B$_4$ - labeled capillary in a human cortical slice, with two pericyte somata (arrow heads) outlined by their basement membrane. (**B**) Pericyte labeled with antibody to PDGFRβ. (**C-D**) Arteriole (**C**) and pericyte (**D**) labeled with isolectin B$_4$ and antibody to α smooth muscle actin (α-SMA, localised in processes originating from the pericyte soma). (**E**) Images of a capillary (red lines indicate diameter) and pericyte soma (arrowheads) in a live human brain slice before drug application (*before*), in the presence of 2 μM superfused noradrenaline (+NA), with 2 μM NA and 500 μM glutamate superfused (+NA +Glu), and after stopping drug superfusion (*washout*). Graph shows time course of capillary diameter at red line throughout the experiment. (**F**) Mean (±s.e.m) glutamate-evoked dilation and noradrenaline-evoked constriction in experiments as in (E) (number of pericytes on bars; change in diameter was quantified relative to that before application of each drug; relative to the pre-noradrenaline diameter the glutamate-evoked dilation was 26.8±7.7%). (**G**) Silver staining of an SDS-PAGE gel for Aβ solutions prepared as in the Materials and Methods. (**H**) Images of a human capillary before and after superfusion of 72 nM Aβ$_{1-42}$, showing a region (red line) being constricted by a pericyte (arrowheads). Graph shows mean (±s.e.m) diameter change at 4 pericyte locations from 4 slices treated with Aβ and 3 pericyte locations from 3 slices superfused with aCSF lacking Aβ (significantly reduced at 40 mins in Aβ, p=0.01).
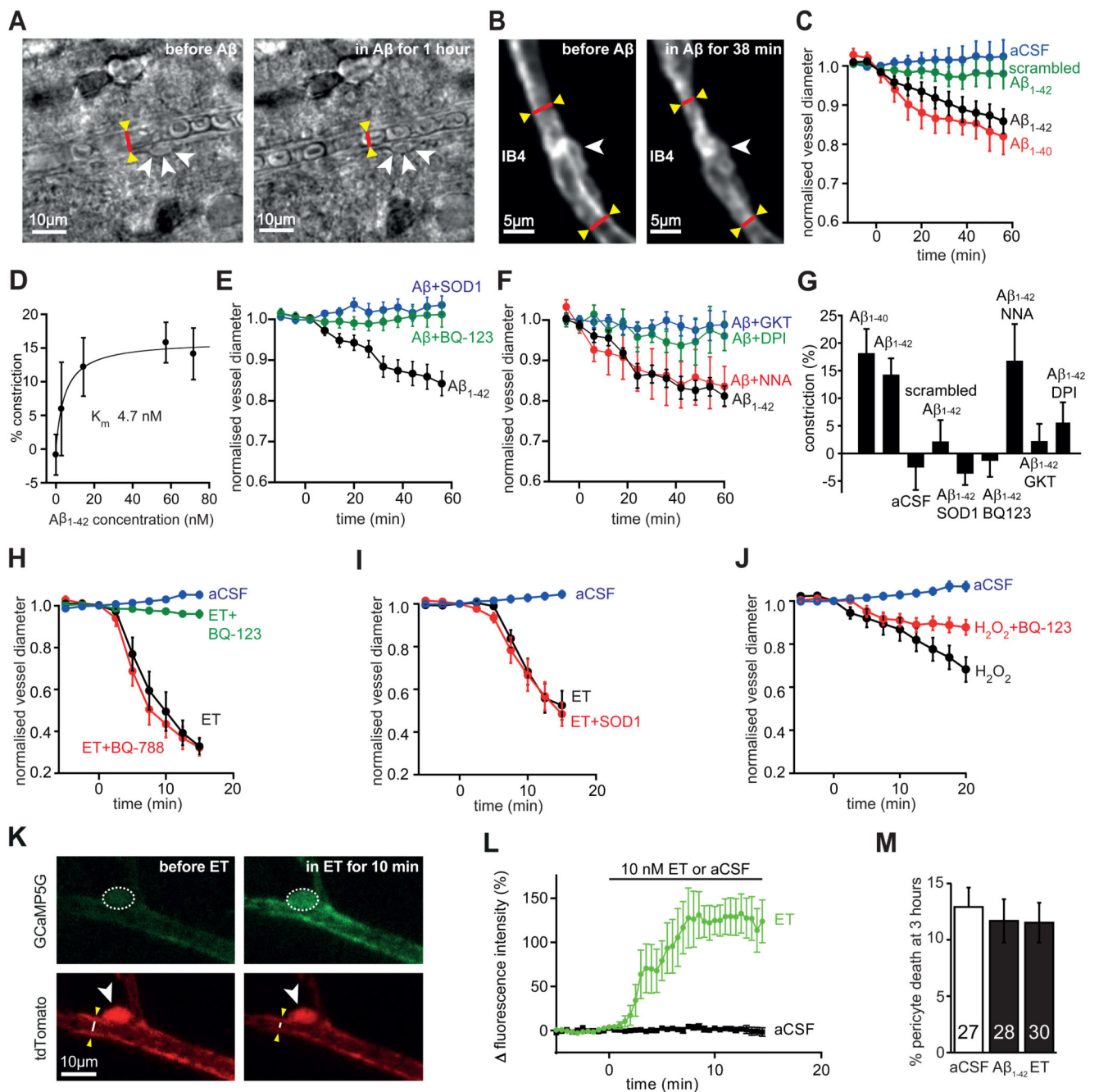
Figure 2. Aβ acts via reactive oxygen species and endothelin type A receptors.
(**A-B**) Bright field images (**A**) and two-photon evoked IB_4 fluorescence (**B**) of capillaries in rat cortical slices in aCSF and after applying 72 nM $Aβ_{1-42}$, showing constriction near pericytes (arrowheads, cf. Figs. S2, S3). (**C**) Mean (±s.e.m) time course of capillary diameter during superfusion with aCSF (n=51 vessels), scrambled $Aβ_{1-42}$ (109 nM, n=32), $Aβ_{1-42}$ (72 nM, n=20) or $Aβ_{1-40}$ (100 nM, n=6). (**D**) Constriction evoked after 1 hour by different concentrations of $Aβ_{1-42}$ (n=51, 11, 10, 19 and 20 for 0, 2.9, 14, 57 and 72 nM respectively). Curve is a Michaelis-Menten relation with a K_m of 4.7 nM and a maximum of 16.1%. (**E-J**)

Time course of diameter when applying the following agents (experiments on each figure panel were interleaved; blockers were present for 5-15 mins before Aβ). (**E**) 57 nM Aβ$_{1-42}$ alone (n=19), or in the presence of superoxide dismutase 1 (SOD1, 150 units/ml, n=19) or the ET$_A$ blocker BQ-123 (1 μM, n=14). (**F**) 72 nM Aβ$_{1-42}$ alone (n=7), or in the presence of the NOS blocker L-NNA (100 μM, n=6), the NADPH oxidase blocker DPI (10 μM, n=5), or the NOX4 blocker GKT137831 (0.45 μM, n=7). (**G**) Constriction produced at 60 mins for (C)-(F). (**H**) Effect of aCSF (n=10), ET alone (10 nM, n=10), or ET in the presence of the ET$_A$ blocker BQ-123 (1 μM, n=10) or the ET$_B$ blocker BQ-788 (1 μM, n=12). (**I**) aCSF or ET (5 nM) in the absence (n=12) or presence of SOD1 (150 units/ml, n=8). (**J**) aCSF or the ROS generator H$_2$O$_2$ (1 mM, n=9, which evokes constriction: p=1.1x10^{-5} at 20 mins) or H$_2$O$_2$ with the ET$_A$ blocker BQ-123 (1 μM, n=11, constriction is reduced, p=0.009). (**K**) Two-photon image of mouse cortical pericyte expressing GCaMP5G (green), before and while applying ET (10 nM), which raises [Ca^{2+}]$_i$ (increase in green intensity) in pericyte soma (arrowhead, dashed line shows ROI analysed) and processes, and constricts the capillary (see white line on image of the tdTomato reporter of GCaMP5G expression, red). (**L**) Mean [Ca^{2+}]$_i$ time course in 8 pericyte somata in response to ET (significantly elevated, p=0.0014) and in 7 somata in aCSF (no significant change, p=0.74). (**M**) Incubating rat brain slices (number on bars) with Aβ$_{1-42}$ oligomers (1.4 μM) or ET (100 nM) for 3 hours does not increase pericyte death.
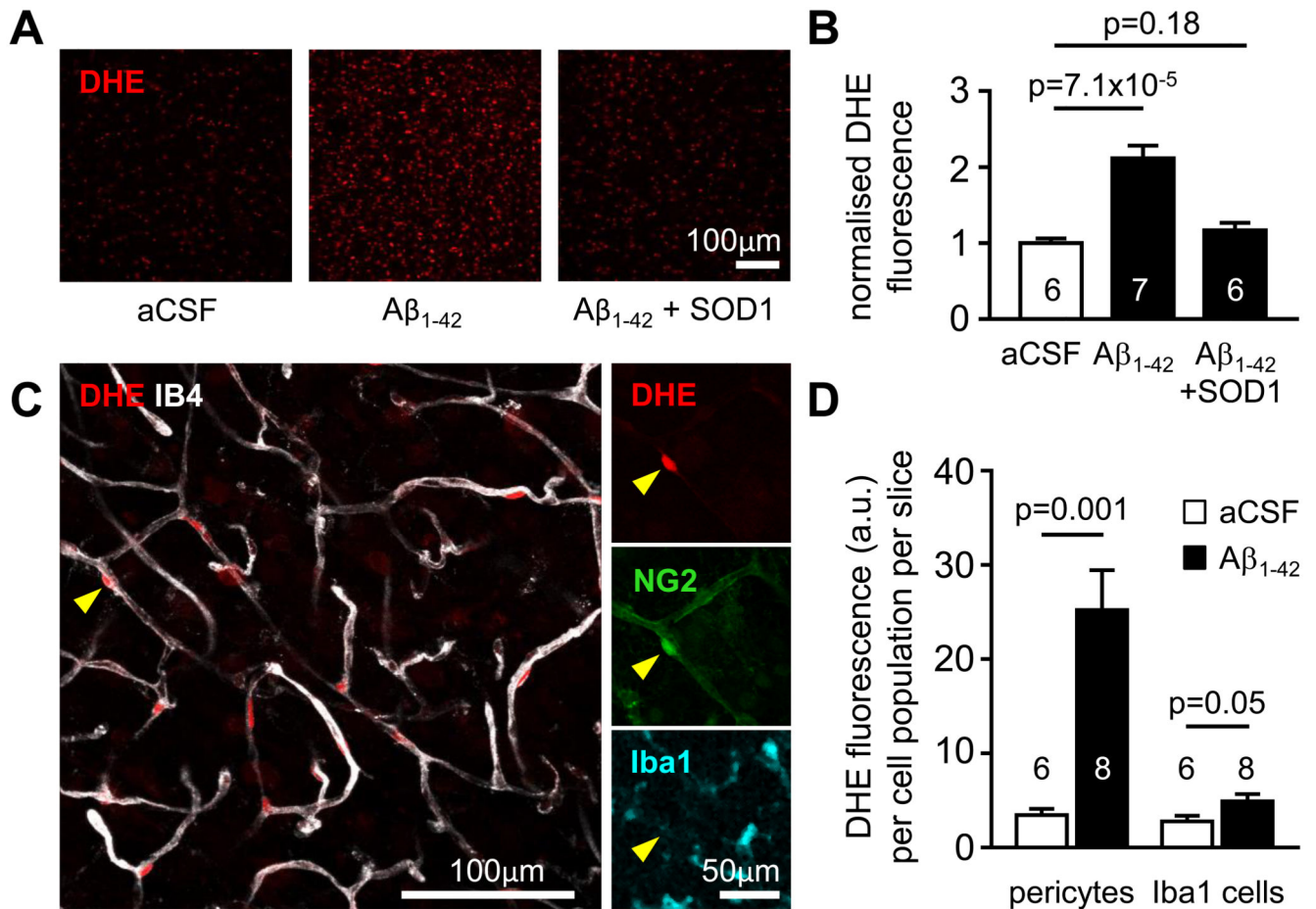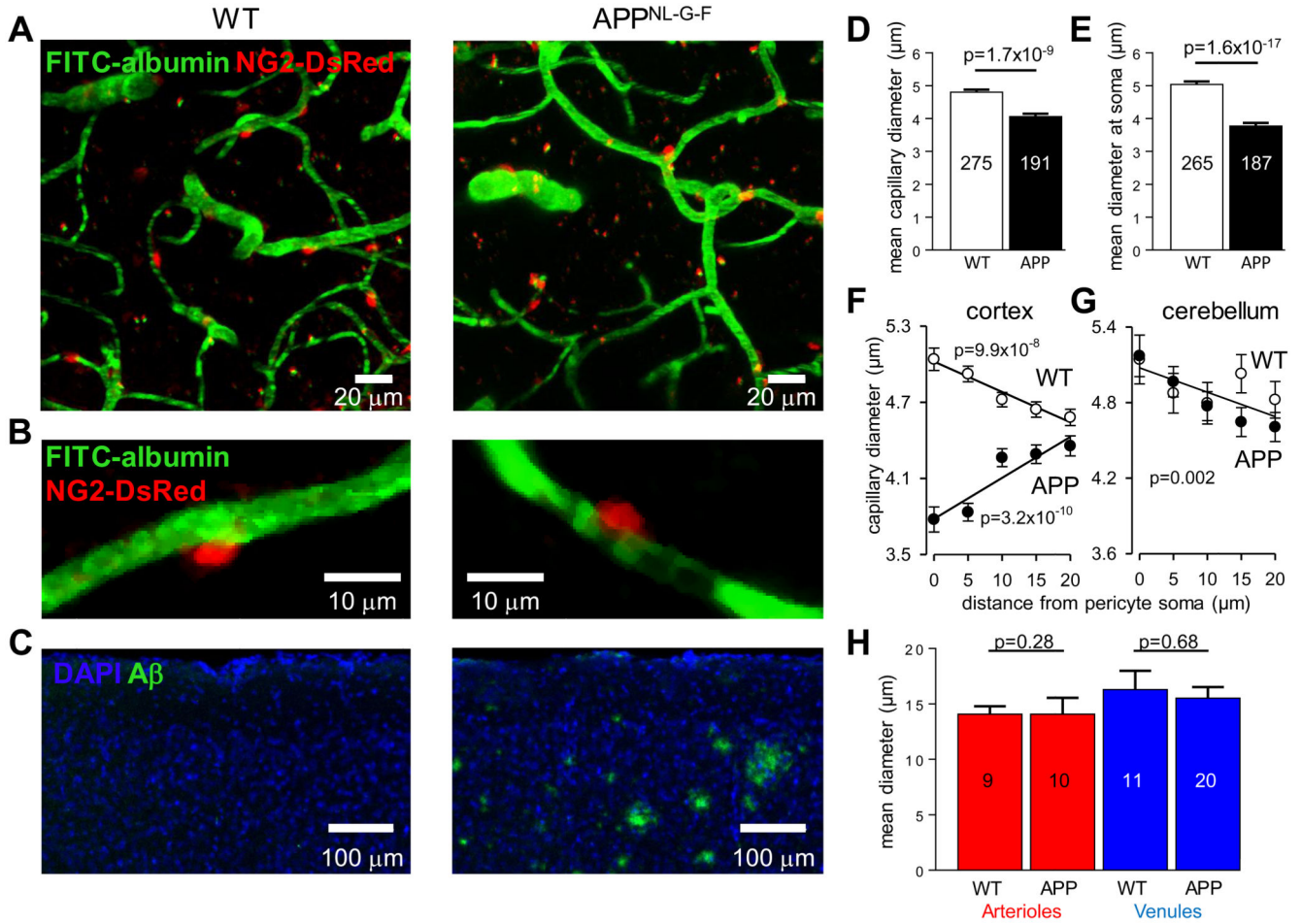
Figure 3. Aβ evokes ROS generation in pericytes.
(**A**) Fluorescence images of dihydroethidium (DHE) loaded rat cortical slices incubated in control aCSF or aCSF containing $A\beta_{1-42}$ (72 nM) or $A\beta_{1-42}$ + SOD1 (150 units/ml) for 40 min, showing that Aβ increases ROS level, and this is inhibited by SOD1. (**B**) Fluorescence (normalised to value in aCSF, mean±s.e.m.) of slices incubated in aCSF (n=6), $A\beta_{1-42}$ (n=7) or $A\beta_{1-42}$ + SOD1 (n=6). (**C**) Left: Image of a cortical slice showing that the brightest DHE-labeled cells are located on IB_4-labeled blood vessels (arrowhead). Right: Immunolabeling shows that these cells colocalise with NG2, but not Iba1, implying that they are pericytes rather than microglia or perivascular macrophages. (**D**) Soma DHE fluorescence (arbitrary units (a.u.), mean±s.e.m.) from the population of pericytes, or of Iba1-labeled cells, after 40 mins in the absence or in the presence of $A\beta_{1-42}$. Numbers on bars are slices (fluorescence was averaged across 3 image stacks for each slice).
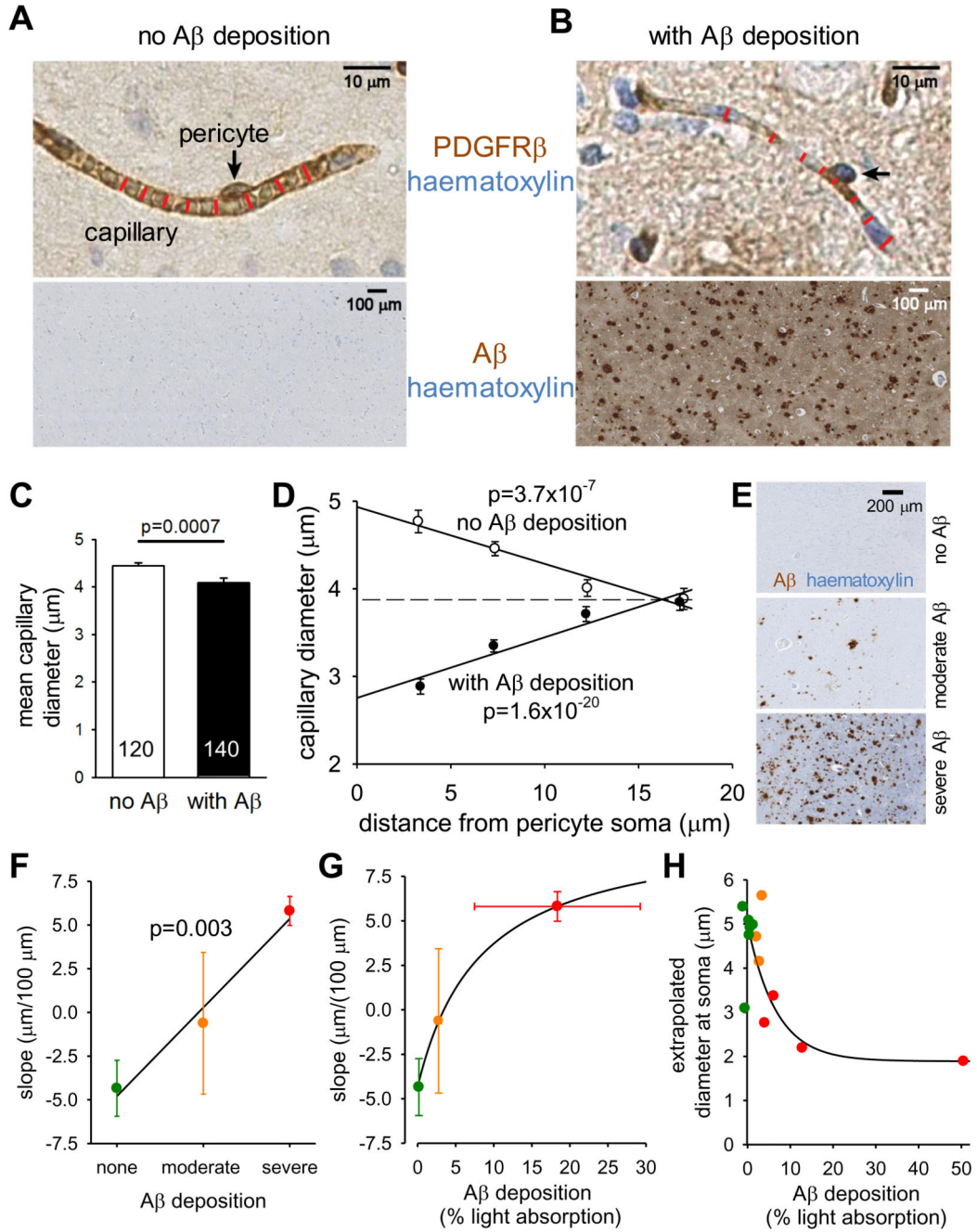
Figure 4. Pericyte-mediated capillary constriction occurs in humans with Aβ deposits.
(**A-B**) Specimen images of human cortical biopsies, labeled for PDGFRβ (brown in top panels) to show pericytes (arrows), from patients lacking (**A**) or exhibiting (**B**) Aβ deposits (brown in bottom panels, haematoxylin counterstain blue). Red lines indicate capillary diameter. (**C**) Mean (±s.e.m) diameter of capillaries in patients lacking (3921 diameters measured) or exhibiting (5121 diameters measured) Aβ deposits (number of images analysed shown on bars). (**D**) Dependence of capillary diameter on distance from a visible pericyte soma (in 5 μm bins, from 0-5, 5-10, 10-15 and 15-20 μm, plotted at the mean

distance for each bin) for patients lacking or exhibiting Aβ deposits (moderate and severe Aβ deposition pooled together). P values assess whether slope of regression line is significantly different from zero. (**E**) Examples of Aβ labeling assessed by the neuropathologist as absent, moderate or severe. (**F**) Slope of regression lines as in (D) plotted as a function of neuropathologist-rated parenchymal Aβ load for each biopsy (n=6 biopsies for none, n=3 for moderate, n=4 for severe). P value compares slope of line with zero. (**G**) Slope of regression lines as in (D) plotted as a function of severity of Aβ deposition measured optically for each biopsy, with subjects grouped by colour (defined in (F)) as classified by neuropathologist. (**H**) Dependence of extrapolated diameter at soma (as in (D)) on severity of Aβ deposition measured optically for each biopsy, with subject points coloured as classified by neuropathologist (defined in (F)). Lines through data in (F)-(H) show the trends in the data.

Diameters were assessed at depths that did not differ significantly: 158.4±6.7 μm and 131.9±5.0 μm (p=0.23 by Mann-Whitney test) for neocortical capillaries, 142±26 μm and 137±21 μm (p=0.88) for arterioles, and 85±15 μm and 89±9 μm (p=0.81) for venules, in WT and AD mice respectively.
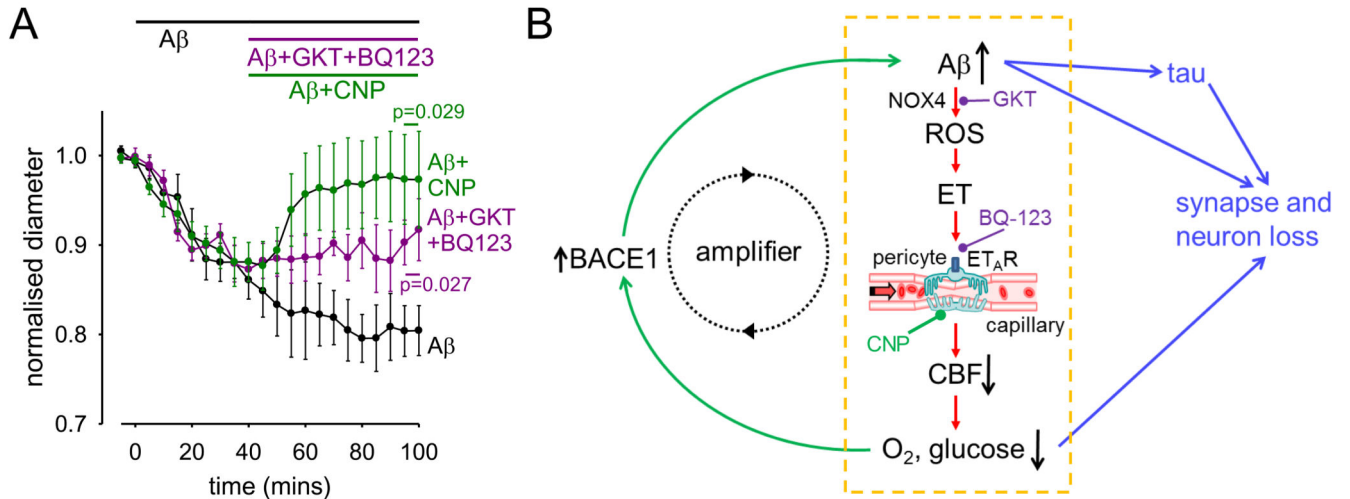
Figure 6. Aβ effects on capillaries may amplify the onset of AD, and are reversible.
(**A**) Applying GKT137831 (0.45 μM) to block NOX4 and BQ-123 (1 nM) to block ET_ARs, or C-type natriuretic peptide (CNP, 100 nM, see Fig. S8), significantly reduced the constriction evoked by Aβ (72 nM, p=0.027 and 0.029 respectively, corrected for multiple comparisons, data are presented as mean±s.e.m.). (**B**) Summary of our results and their implications. Our data reveal the pathway within the yellow dashed box. Amyloid β oligomers activate NADPH oxidase 4 in pericytes to generate reactive oxidative species (ROS). These in turn release, or potentiate the constricting effects of, endothelin-1 which acts via ET_A receptors on pericytes on capillaries - the locus (16) of the largest component of vascular resistance within the brain parenchyma. Capillary constriction decreases cerebral blood flow and hence the supply of oxygen and glucose to the brain. Green arrows on the left show that this increases the production of Aβ, in part by upregulating (13, 14) expression of β-amyloid converting enzyme (β-secretase 1, BACE1), thus forming an amplifying positive feedback loop. Blue arrows on the right show that a rise in Aβ concentration, either directly, or via downstream tau production, or via the decrease in oxygen and glucose supply, leads to the loss of synapses and neurons. Potential sites for therapeutic intervention are highlighted at the stages of ROS production by NOX4 (GKT), endothelin receptors (BQ-123) and CNP receptors (see also Fig. S8).
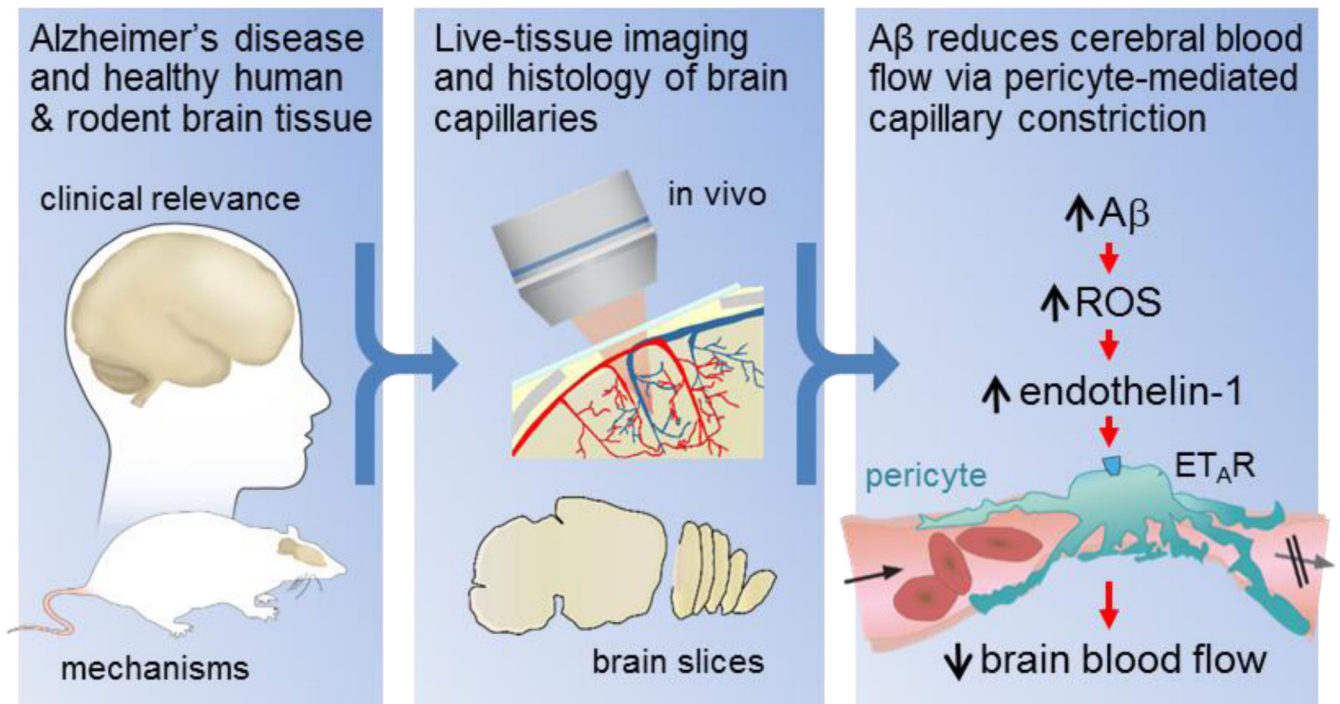
Figure. Live human and rodent brain capillaries become constricted in Alzheimer's disease.
Tissue from humans and rodents (left panel) that were healthy or developing Alzheimer's disease (AD) was imaged *in vivo* and as brain slices (middle panel), revealing that pericytes constrict brain capillaries early in AD via a mechanism involving ROS generation and release of endothelin-1 which activates ET_A receptors (right panel).